

## Article

# Study on Formation Mechanism of Pre-stressed Anchor Pressure Arch Based on Safe Co-Mining of Deep Coal and Gas

Deyi Wu <sup>1,\*</sup>, Nanyu Li <sup>1</sup>, Menghan Hu <sup>1</sup> and Hanghang Liu <sup>2</sup><sup>1</sup> College of Civil Engineering, Anhui Jianzhu University, Hefei 230601, China<sup>2</sup> Anhui Construction Engineering Quality Second Supervision and Inspection Station, Hefei 230000, China

\* Correspondence: wudeyi136@163.com; Tel.: +86-151-5601-0510

**Abstract:** It is challenging to assure safe and effective gas mining due to the surrounding soft coal rock and rock roads in deep and high gas mines being extremely loose and broken. One of the effective ways is to arrange pre-stressed anchors in a certain area of the roadway surrounding rocks to form a compression arch with the joint action of anchors and surrounding rocks, but due to the lack of in-depth systematic research on the formation mechanism of the compression arch, the effect is difficult to give full play. The typical microstructure of deep soft coal and rock was observed by the borehole camera method, and the mechanical performance parameters were measured in the laboratory. The distribution characteristics of different bolt spacing, bolt pre-tightening force, and bolt length along the bolt arrangement direction and the additional compressive stress on the surface of the straight wall of a semi-circular arch deep soft coal and rock roadway were numerically simulated and analyzed. According to the uniform distribution range and size of the small fluctuation of the additional compressive stress inside the coal and rock, the distribution and size of the additional compressive stress on the surface of the straight wall and the effective superposition of the additional compressive stress, and the thickness and strength of the compression arch of the deep coal and rock preload bolt were analyzed, and the reasonable parameters of the pre-stressed bolt were determined. The results show that bolt spacing, pre-tightening force, and bolt length significantly affect the thickness and strength of the compression arch. The reasonable spacing of the pre-stressed bolt was  $a \times b = 600 \text{ mm} \times 600 \text{ mm} \sim 400 \text{ mm} \times 400 \text{ mm}$ , the pre-stressed bolt pre-tightening force was  $F = 50 \sim 90 \text{ kN}$ , the length of the pre-stressed bolt was  $L = 1500 \sim 2000 \text{ mm}$ , the strength of compression arch was  $\Delta\sigma_c = -1.480 \sim -1.589 \text{ MPa}$ , and the thickness of the compression arch was  $m = -266.67 \sim -533.33 \text{ mm}$ .

**Keywords:** gas safe and efficient mining; deep soft rock roadway; parameters of the pre-stressed bolt; thickness of the pre-stressed bolt compression arch; strength of the pre-stressed bolt compression arch



**Citation:** Wu, D.; Li, N.; Hu, M.; Liu, H. Study on Formation Mechanism of Pre-stressed Anchor Pressure Arch Based on Safe Co-Mining of Deep Coal and Gas. *Sustainability* **2023**, *15*, 3004. <https://doi.org/10.3390/su15043004>

Academic Editor: Rajesh Kumar Jyothi

Received: 27 November 2022

Revised: 31 January 2023

Accepted: 2 February 2023

Published: 7 February 2023



**Copyright:** © 2023 by the authors. Licensee MDPI, Basel, Switzerland. This article is an open access article distributed under the terms and conditions of the Creative Commons Attribution (CC BY) license (<https://creativecommons.org/licenses/by/4.0/>).

## 1. Introduction

In China, 70% of coal resources are located in the deep part [1] and the deep coal seam is endowed with gas [2]; the extraction schematic diagram is shown in Figure 1. Digging the gas extraction roadway [3] and setting up the coal seam drilling and gas extraction equipment for coal seam gas extraction not only efficiently reduces the coal seam gas content and ensures the safety of coal seam mining, but also fully utilizes the function of coal seam gas as a civil fuel. However, due to the poor lithology of the surrounding rock, significant ground stress, and complex tectonics, the surrounding rock is significantly loosened and broken after excavation of the deep extraction roadway [4]; the phenomenon of “destabilization” of the surrounding rock is common, with roof erosion and flaky gang occurring from time to time, making it difficult to install and use the gas extraction facilities in the roadway normally and ensure efficient and safe gas extraction. In order to effectively solve the above problems, the project team proposed the method of forming a compression arch in a certain area of the roadway surrounding rock to ensure the stability of the roadway surrounding rock and the smooth extraction of gas. This study has wide applicability for

gas extraction in deep soft coal rock roadway, but it is not suitable for gas extraction in shallow hard rock roadway.

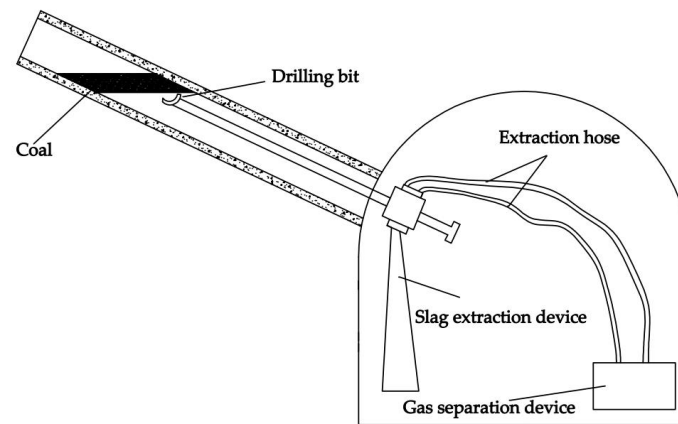


**Figure 1.** Gas Extraction Diagram.

As shown in Figure 2, the pre-stressed bolts are arranged immediately after the excavation of the roadway. The pre-stressed force of a single bolt forms a triangular distribution of additional compressive stress in the surrounding rock, and the row spacing between bolts is reasonably selected to make the additional compressive stress in the surrounding rock effectively superimposed, forming a certain range of uniformly distributed additional compressive stress; the appropriate size of additional compressive stress can cause the strength of the surrounding rock to effectively increase, forming a certain thickness and strength compression arch. Then, auxiliary pre-stressed anchor cables, grouting, and metal scaffold and other combined support carry the load together to keep the surrounding rock of the deep soft rock roadway stable [5–9], so that coal and gas can be extracted together. The application in the project has achieved satisfactory results. However, due to the loose structure of coal rock in the project and more micro-cracks, conventional support theories such as suspension theory, combined beam theory, and surrounding rock reinforcement theory are no longer applicable [10–13]. Targeted support theory has not yet been formed, so the selection of support parameters often starts from experience, which is difficult for achieving the expected effect [14,15]. This paper used FLAC3D software, which is a three-dimensional numerical simulation analysis software for continuous media developed by ITASA. Based on the three-dimensional finite difference method, the Lagrange numerical analysis method of the mixed unit discrete model is used to divide the rock mass into many plastic flow bodies, select a reasonable model and appropriate boundary conditions, and simulate and analyze the large deformation, instability, and sliding of the rock mass. The parameters of a pre-stressed bolt include bolt pre-stressed force, bolt length, bolt spacing, type of bolt, the diameter of the bolt, etc. High-strength ribbed steel bolt is generally selected for the pre-stressed bolt and the diameter of the bolt is 14 mm. Through the software simulation, the influence of bolt pre-tightening force ( $F$ ), bolt length ( $L$ ), and spacing of bolt ( $a \times b$ ) support parameters on the distribution of additional compressive stress ( $\Delta\sigma_c$ ) in the surrounding rock [16–20] were analyzed. Combined with experimental research, the influence of compression arch thickness and strength is further analyzed. On this basis, revealing the mechanism of compression arch formation, the research results can provide a basis for the selection of deep soft coal rock support parameters. However, the thickness and strength of the compression arch under different conditions needs to be studied further.

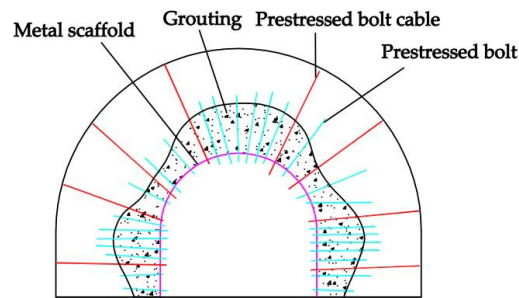


Figure 2. Schematic of the roadway support measure.

## 2. Structure and Mechanical Performance of Coal Rocks

### 2.1. Microstructure of Coal Rocks

Figure 3 shows SEM images of coal rock samples from boreholes in the field. It is observed that there are significant cracks and pores of different sizes on the surfaces of the samples. These pores significantly reduce rock strength and may lead to early failures.

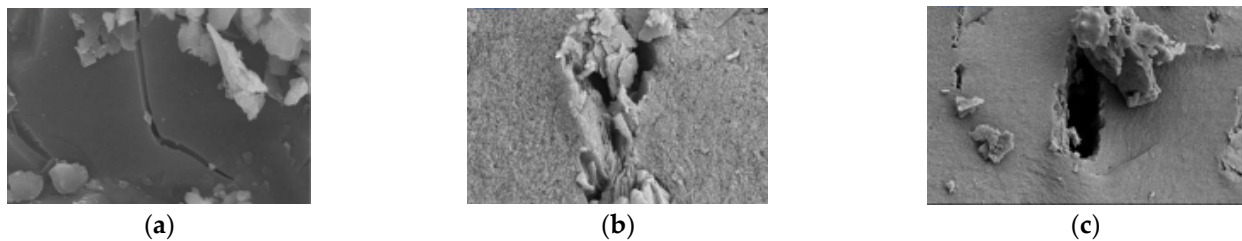


Figure 3. Microstructure of coal rock. (a) Coal sample one, (b) Coal sample two, (c) Coal sample three.

### 2.2. Boreholes of Coal Rock Structures

Figure 4 shows the microstructure of coal rock at different distances ( $S$ ) from the roadway surface in a typical deep coal rock roadway. The obtained images from a borehole camera indicate that the surrounding rock structure of deep soft coal rock roadway is loose, and it is obviously loose and broken in a large range, with a range of about 3.5 m. The vertical and horizontal microcracks are densely distributed and the mechanical properties of coal rock are low.

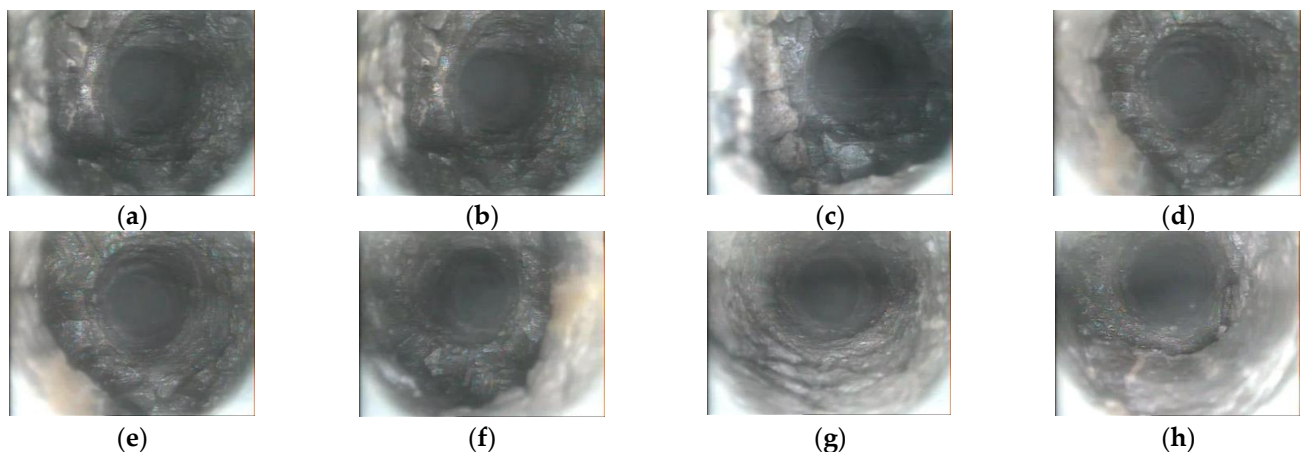


Figure 4. Microstructure of the surrounding rock in a typical coal rock roadway. (a)  $S = 0.5$  m, (b)  $S = 0.8$  m, (c)  $S = 1.2$  m, (d)  $S = 1.5$  m, (e)  $S = 2.0$  m, (f)  $S = 2.5$  m, (g)  $S = 3.0$  m, (h)  $S = 3.5$  m.

### 2.3. Measurement of Mechanical Parameters of the Coal Rock

As shown in Figure 5a, cores were taken from five different parts of the site, three groups for each part, and three specimens for each group. The loose coal rock is made

into standard briquette specimens. The cohesive force ( $c$ ) and internal friction angle ( $\varphi$ ) of coal rock are measured by a YDS soil mechanical property multifunctional tester in Figure 5b, and the elastic modulus ( $E$ ) and Poisson's ratio ( $\gamma$ ) of coal rock are measured by a rock triaxial shear composite testing machine in Figure 5c. The shear modulus ( $G$ ) can be calculated through the following expression. The measured results are shown in Table 1.

$$G = \frac{E}{2(1 + \gamma)}$$

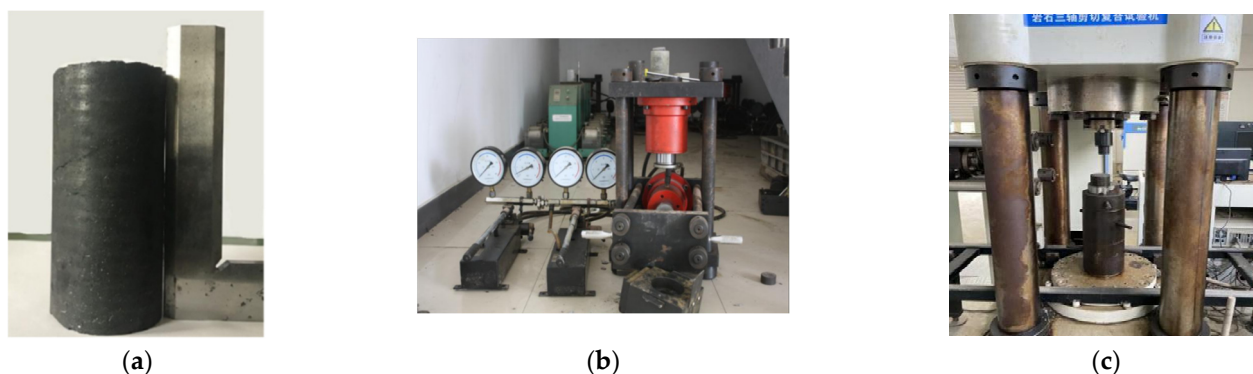


**Figure 5.** Configuration of the test setup and briquette specimen. (a) Prepared standard briquette specimen; (b) YDS soil mechanical performance test apparatus; (c) Rock triaxial testing apparatus.

**Table 1.** Mechanical parameters of typical coal rocks.

Cohesion $c$ (MPa)	Internal Friction Angle $\varphi$	Poisson's Ratio $\gamma$	Elastic Modulus $E$ (MPa)	Shear Modulus $G$ (MPa)
0.5	16	0.36	952	350

### 3. Numerical Model

Figure 6 shows that a semi-circular arch straight wall model with a length, width, and thickness of 60 m, 60 m, and 0.8 m and a 5.2 m  $\times$  1.4 m roadway section was selected as the research object. The roadway was horizontally fixed on both sides and vertically fixed on the bottom. Since the present study was mainly focused on the additional compressive stress ( $\Delta\sigma_c$ ) in the surrounding rock from bolt pre-tightening force, it was assumed that the top of the roadway was free and there was no vertical earth pressure [11]. Two original grid shapes of radial-cylinder and radial-tunnel in the grid prototype library of FLAC3D software were used to establish the grid model of a radial gradient straight wall semi-circular arch roadway. The M-C Mohr-Coulomb model was selected as the constitutive relationship to simulate the additional stress field in surrounding rock. The excavation of the roadway was simulated by the null unit and the support of bolt after excavation of the roadway was simulated by the cable unit. The lithology of a typical coal rock was considered for the surrounding rock, which is a widely adopted technique in simulations. Table 1 presents the mechanical parameters of a typical rock.

The high-strength bolt with an elastic modulus  $E = 100$  GPa, tensile strength  $\delta_s = 490$  MPa, and diameter  $d = 14$  mm was used in the tests and calculations. Meanwhile, different values were considered for the bolt pre-tightening force  $F$  (50, 70, and 90 kN), bolt length  $L$  (1500, 2000, and 2400 mm), and spacing of the bolt  $a \times b$  (400 mm  $\times$  400 mm, 500 mm  $\times$  500 mm, 600 mm  $\times$  600 mm, and 800 mm  $\times$  800 mm) to investigate the additional stresses along the a–A, b–B, c–C, and d–D directions on a typical surrounding rock of roadway and along the a–d direction on the surface of the straight wall.

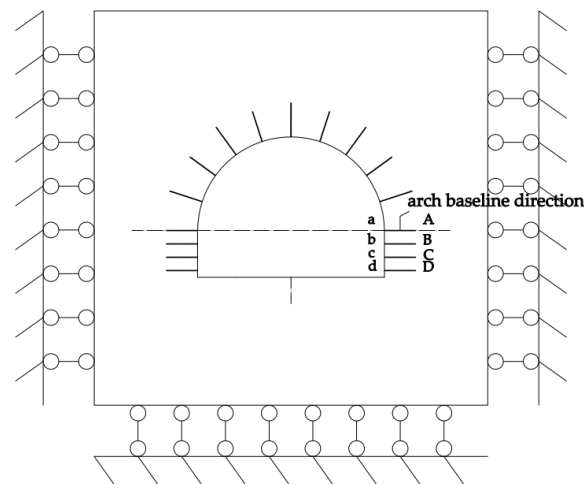


Figure 6. Calculation model.

#### 4. Calculation Results by Numerical Model and Theoretical Analysis

##### 4.1. Magnitude and Distribution of Additional Stress in the Surrounding Rock under Different Bolt Spacing

Figures 7–9 show the distribution of additional stress in the surrounding rock under a pre-tightening force  $F = 70$  kN, bolt length  $L = 2400$  mm, and different bolt spacing, including  $a \times b = 800$  mm  $\times$  800 mm, 600 mm  $\times$  600 mm, 500 mm  $\times$  500 mm, and 400 mm  $\times$  400 mm.

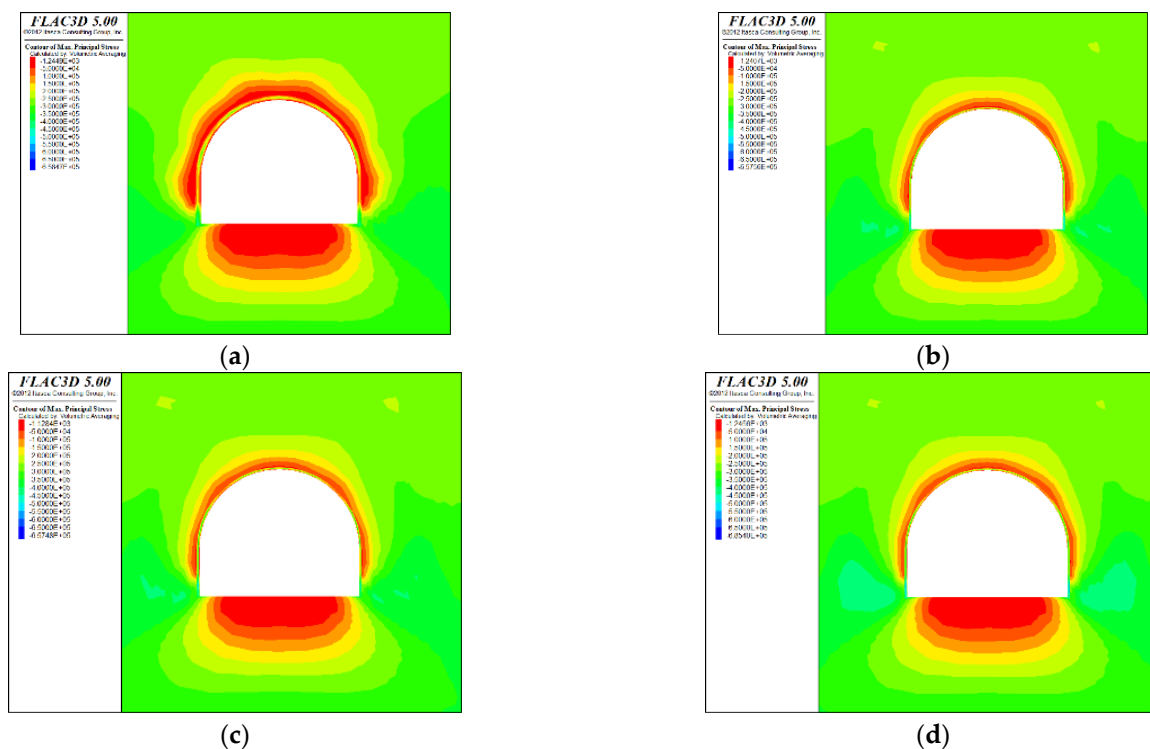
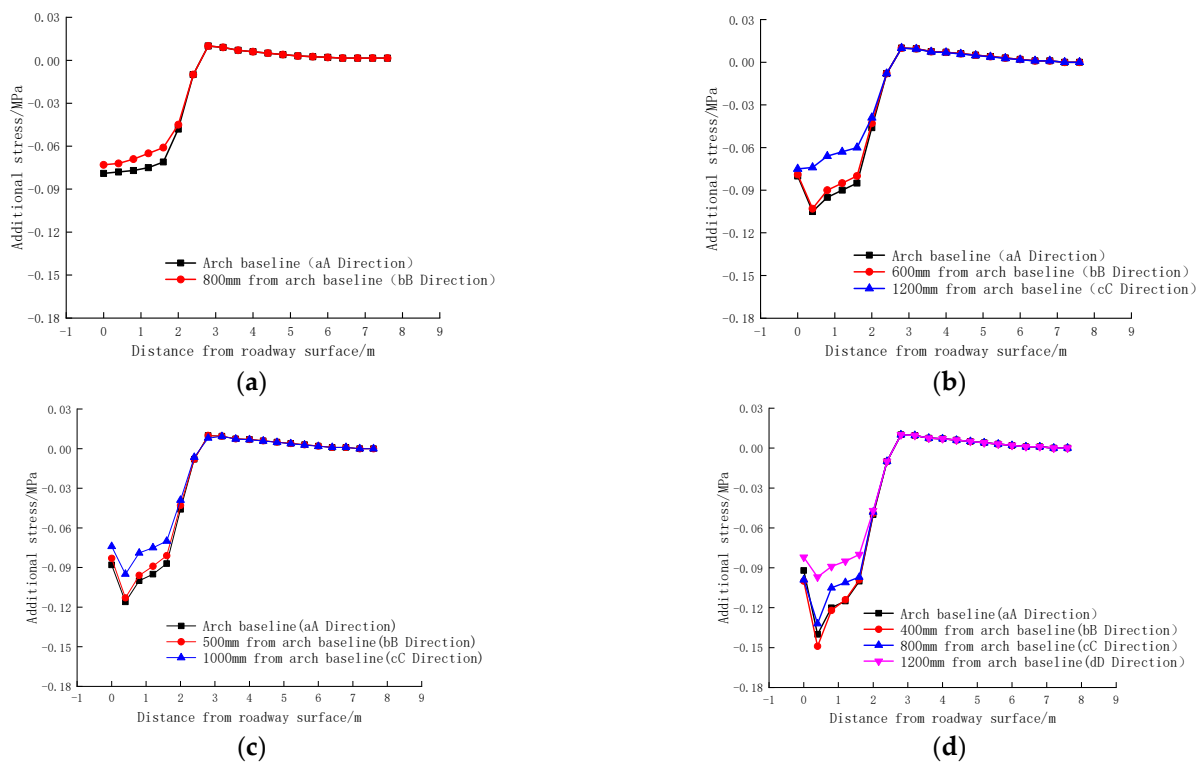
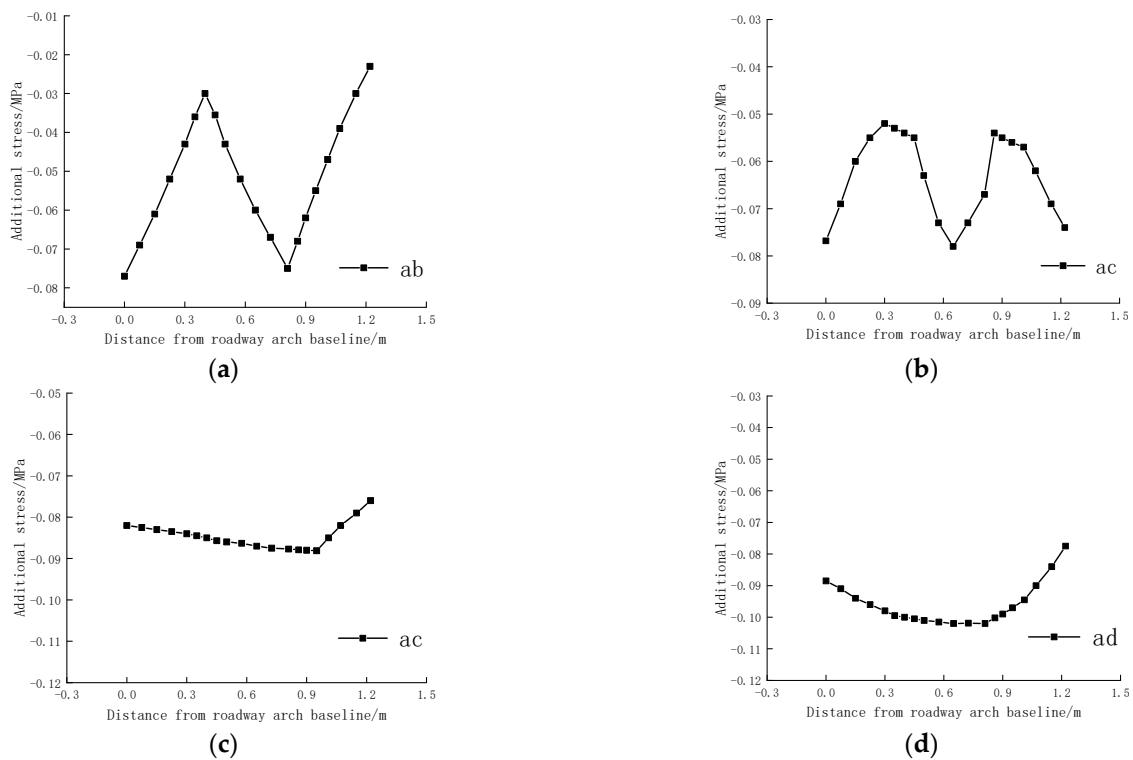


Figure 7. Contours of additional stress in surrounding rock under different bolt spacing. (a) 800 mm  $\times$  800 mm, (b) 600 mm  $\times$  600 mm, (c) 500 mm  $\times$  500 mm, (d) 400 mm  $\times$  400 mm.



**Figure 8.** Distribution of the additional stress in typical parts of the surrounding rock under different bolt spacing. (a) 800 mm × 800 mm, (b) 600 mm × 600 mm, (c) 500 mm × 500 mm, (d) 400 mm × 400 mm.



**Figure 9.** Distribution of the additional stress on the surface of a straight wall under different bolt spacing. (a) 800 mm × 800 mm, (b) 600 mm × 600 mm, (c) 500 mm × 500 mm, (d) 400 mm × 400 mm.

The above results show that:

- (1) Different bolt spacing; within a certain range from the surface of the roadway, the additional compressive stress along the direction of the bolt is first distributed in a small ‘fluctuation’. With the increase of distance from the surface of the roadway, the additional compressive stress decreases at a faster rate.
- (2) The bolt spacing is  $a \times b = 800 \text{ mm} \times 800 \text{ mm}$ ; the additional compressive stress on the surface of the straight wall along the roadway decreases first, then increases and then decreases with the increase of the arch baseline distance. The bolt spacing is  $a \times b = 600 \text{ mm} \times 600 \text{ mm}$ ; the additional compressive stress on the surface of the straight wall along the roadway decreases first, then increases, then decreases, and then increases with the increase of the arch baseline distance. The bolt spacing is  $a \times b = 500 \text{ mm} \times 500 \text{ mm}$  and  $a \times b = 400 \text{ mm} \times 400 \text{ mm}$ ; the additional compressive stress on the surface of the straight wall along the roadway increases first and then decreases with the increase of the arch baseline distance.

The distribution of additional compressive stress in the surrounding rock of the roadway with different bolt spacing is shown in Table 2.

**Table 2.** Distribution of the additional compressive stress in the surrounding rock of the roadway with different bolt spacing.

Bolt Spacing $a \times b$ (mm)	$\Delta\sigma_c$ Uniform Distribution Range (mm)	$\Delta\sigma_c$ Distribution Interval (Mpa)				Roadway Straight Wall Surface $\Delta\sigma_c$ Distribution Interval (Mpa)
		aA Direction	bB Direction	cC Direction	dD Direction	
800 × 800	1600	−0.071~−0.078	−0.061~−0.073	-	-	−0.021~−0.076
600 × 600	1600	−0.08~−0.105	−0.079~−0.103	−0.06~−0.075	-	−0.052~−0.078
500 × 500	1600	−0.087~−0.116	−0.081~−0.113	−0.07~−0.095	-	−0.078~−0.089
400 × 400	1600	−0.092~−0.115	−0.099~−0.149	−0.097~−0.132	−0.08~−0.097	−0.078~−0.102

#### 4.2. Magnitude and Distribution of Additional Stress in the Surrounding Rock at Different Bolt Pre-Tightening Force

After presenting the results of the simulation with a bolt length  $L$  of 2400 mm, bolt spacing  $a \times b$  of 400 mm × 400 mm, and bolt pre-tightening force  $F$  of 70 kN, the following results were obtained based on simulations with a bolt pre-tightening force  $F$  of 50 and 90 kN. The distribution of additional stress in the surrounding rock is shown in Figures 10–12.

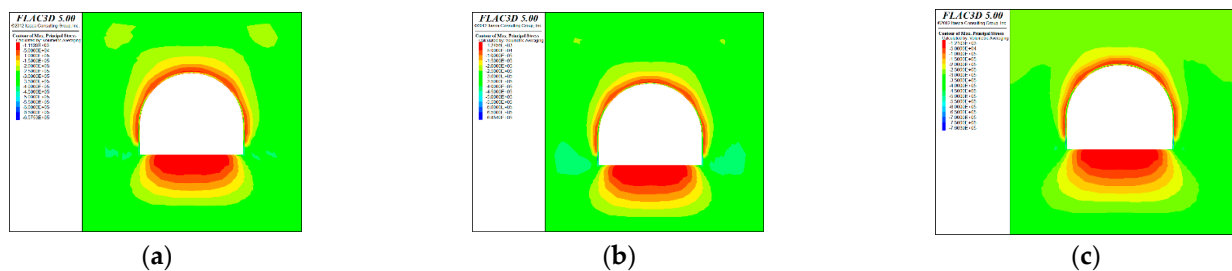


**Figure 10.** Contours of additional stress in the surrounding rock under different bolt pre-tightening force. (a)  $F = 50 \text{ kN}$ , (b)  $F = 70 \text{ kN}$ , (c)  $F = 90 \text{ kN}$ .

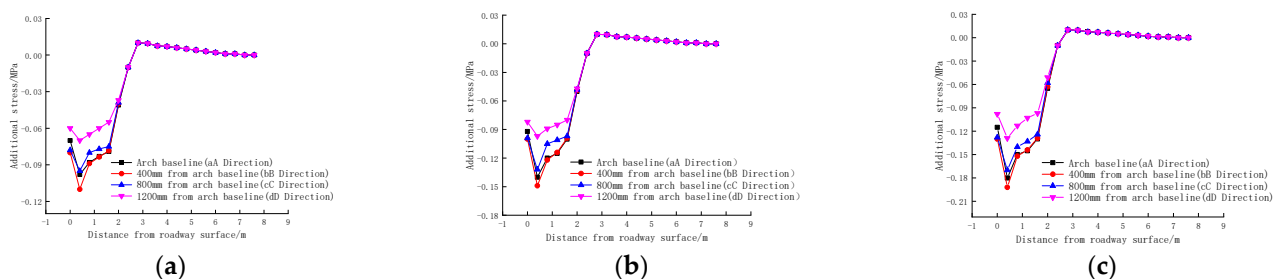


**Figure 11.** Distribution of additional stress in typical parts of the surrounding rock under different bolt pre-tightening force. (a)  $F = 50 \text{ kN}$ , (b)  $F = 70 \text{ kN}$ , (c)  $F = 90 \text{ kN}$ .

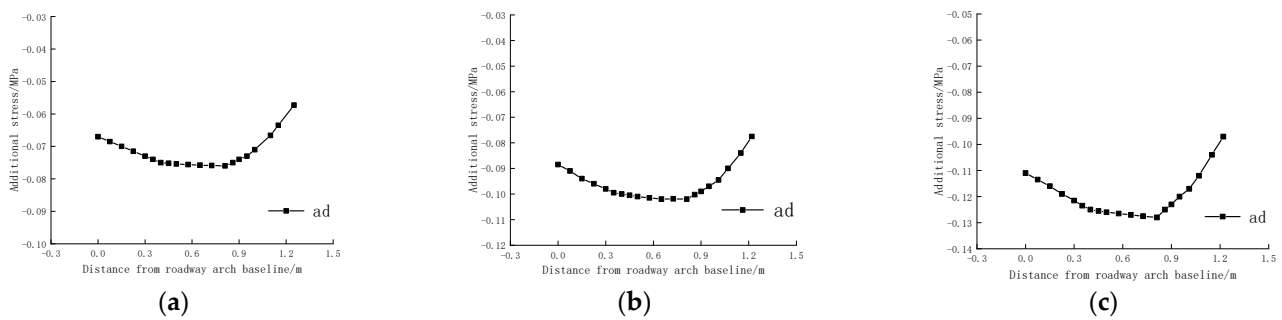


**Figure 12.** Distribution of additional stress on the surface of the straight wall under different bolt pre-tightening force. (a)  $F = 50$  kN, (b)  $F = 70$  kN, (c)  $F = 90$  kN.

The above results show that:

- (1) Different bolt pre-tightening force; within a certain range from the surface of the roadway, the additional compressive stress along the direction of the bolt is first distributed in a small ‘fluctuation’. With the increase of distance from the surface of the roadway, the additional compressive stress attenuates at a faster rate.
- (2) The bolt pre-tightening force  $F = 50$  kN,  $F = 70$  kN, and  $F = 90$  kN; the additional compressive stress along the surface of the straight wall of the roadway increases first and then decreases with the increase of the arch baseline distance.

The distribution of the additional compressive stress in the surrounding rock of the roadway with different bolt pre-tightening force is shown in Table 3.

**Table 3.** Distribution of the additional compressive stress in the surrounding rock of the roadway with different bolt pre-tightening force.

Bolt Pre-Tightening Force $F$ (kN)	$\Delta\sigma_c$ Uniform Distribution Range (mm)	$\Delta\sigma_c$ Distribution Interval (Mpa)				Roadway Straight Wall Surface $\Delta\sigma_c$ Distribution Interval (Mpa)
		aA Direction	bB Direction	cC Direction	dD Direction	
50	1600	-0.07~ -0.098	-0.079~ -0.11	-0.075~ -0.095	-0.055~ -0.07	-0.057~ -0.076
70	1600	-0.092~ -0.115	-0.099~ -0.149	-0.097~ -0.132	-0.08~ -0.097	-0.078~ -0.102
90	1600	-0.115~ -0.18	-0.129~ -0.192	-0.124~ -0.17	-0.097~ -0.098	-0.097~ -0.128

### 4.3. Magnitude and Distribution of Additional Stress in the Surrounding Rock under Different Bolt Lengths

After presenting the results of the simulation with a bolt length  $L$  of 2400 mm, bolts spacing  $a \times b$  of 400 mm  $\times$  400 mm, and bolt pre-tightening force  $F$  of 70 kN, the following results were obtained based on simulations with bolt length  $L$  of 1500 and 2000 mm. The distribution of additional stress in surrounding rock is reported in Figures 13–15.

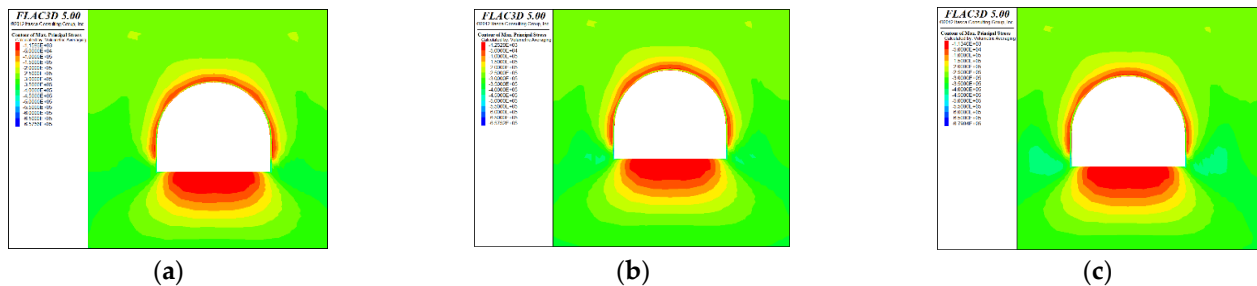


**Figure 13.** Contours of additional stress in the surrounding rock under different bolt lengths. (a)  $L = 1500$  mm, (b)  $L = 2000$  mm, (c)  $L = 2400$  mm.

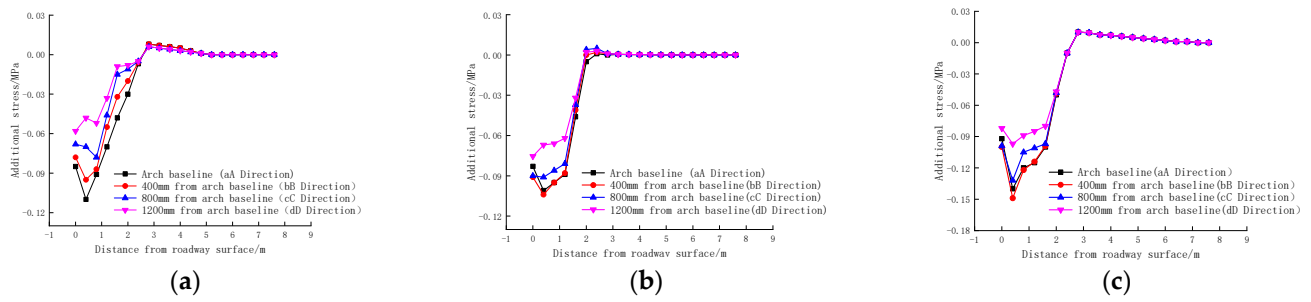


Figure 14. Distribution of additional stress in typical parts of the surrounding rock under different bolt lengths. (a) L = 1500 mm, (b) L = 2000 mm, (c) L = 2400 mm.

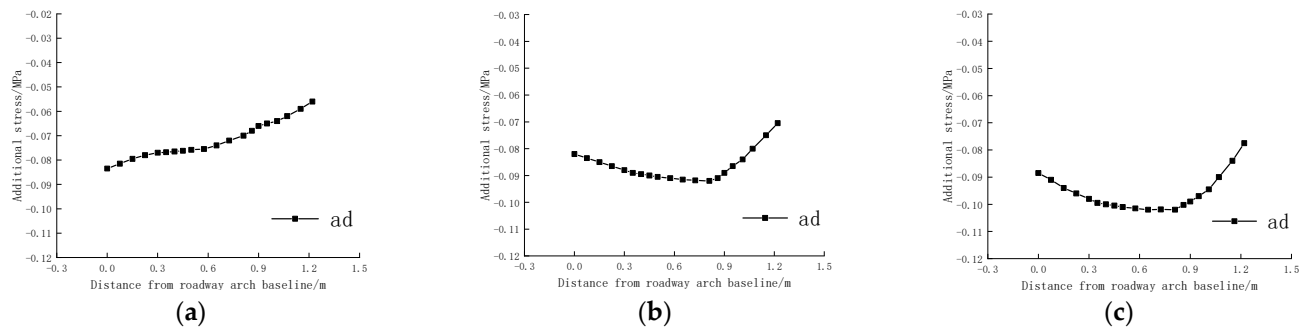


Figure 15. Distribution of additional stress on the wall surface along the a-d direction under different bolt lengths. (a) L = 1500 mm, (b) L = 2000 mm, (c) L = 2400 mm.

The above results show that:

- (1) Different bolt length; within a certain range from the surface of the roadway, the additional compressive stress along the direction of the bolt is first distributed in a small ‘fluctuation’. With the increase of distance from the surface of the roadway, the additional compressive stress attenuates at a faster rate.
- (2) The bolt length L = 1500 mm; the additional compressive stress along the straight wall surface of the roadway decreases with the increase of the arch baseline distance. The bolt length L = 2000 mm and L = 2400 mm; the additional compressive stress on the surface of the straight wall along the roadway increases first and then decreases with the increase of the arch baseline distance.

The distribution of the additional compressive stress in the surrounding rock of the roadway with different bolt length is shown in Table 4.

Table 4. Distribution of the additional compressive stress in the surrounding rock of the roadway with different bolt length.

Bolt Length L (mm)	$\Delta\sigma_c$ Uniform Distribution Range (mm)	$\Delta\sigma_c$ Distribution Interval (Mpa)				Roadway Straight Wall Surface $\Delta\sigma_c$ Distribution Interval (Mpa)
		aA Direction	bB Direction	cC Direction	dD Direction	
1500	800	-0.085--0.11	-0.078--0.095	-0.068--0.078	-0.048--0.058	-0.056--0.084
2000	1200	-0.083--0.101	-0.088--0.104	-0.081--0.091	-0.062--0.076	-0.071--0.092
2400	1600	-0.092--0.115	-0.099--0.149	-0.097--0.132	-0.08--0.097	-0.078--0.102

## 5. Formation and Bearing Mechanism the Pre-Stressed Bolt Compression Arch in a Deep Soft Rock Roadway

### 5.1. Formation of the Pre-Stressed Bolt Compression Arch in a Deep Soft Rock Roadway

Figures 7a, 8a, 9a and 16a reveal that when the bolt spacing  $a \times b$  was set to 800 mm  $\times$  800 mm while the pre-stressed bolts were installed along the b–B and a–A directions, triangular additional compressive stress zones form in the surrounding rock. The additional compressive stress inside the triangle EFG formed by the single pre-stressed bolt along the d–B direction in the surrounding rock was  $\Delta\sigma_c = -0.068$  Mpa. The triangle height of single pretension bolt height H was determined by the range of the uniformly distributed

additional compressive stress with small fluctuations. Accordingly, it was found that  $H = 1600$  mm. Given the relatively small effects of additional compressive stress on increasing the surrounding rock strength when  $\Delta\sigma_c \leq -0.04$  Mpa, the width  $w$  of the bottom side of the triangle EFG could be determined by the range  $\Delta\sigma_c > -0.04$  Mpa. Accordingly, the width was taken as  $w = 600$  mm. Figures 7b, 8b, 9b and 16b reveal that when the bolt spacing  $a \times b$  is decreased to  $600$  mm  $\times$   $600$  m, the height  $H$  of the triangle formed by the single pre-stressed bolt along the b-B direction does not change remarkably, while the additional compressive stress increases from  $\Delta\sigma_c = -0.068$  Mpa to  $\Delta\sigma_c = -0.087$  Mpa; the additional compressive stress zones of triangles formed by the pre-stressed bolts within the radius of  $600$  m along the b-B and a-A directions in the surrounding rock are interconnected, but no superposition is formed. When the bolt spacing  $a \times b$  is further decreased to  $500$  mm  $\times$   $500$  mm and  $400$  mm  $\times$   $400$  mm, the height  $H$  of the triangle formed by the single pre-stressed bolt along the b-B direction in the surrounding rock slightly varies. Meanwhile, the additional compressive stress increases to  $\Delta\sigma_c = -0.092$  Mpa and  $\Delta\sigma_c = -0.117$  Mpa, and the delta additional compressive stress zones of adjacent pre-stressed bolts are superposed and form a compression arch with a certain thickness of  $m$ .

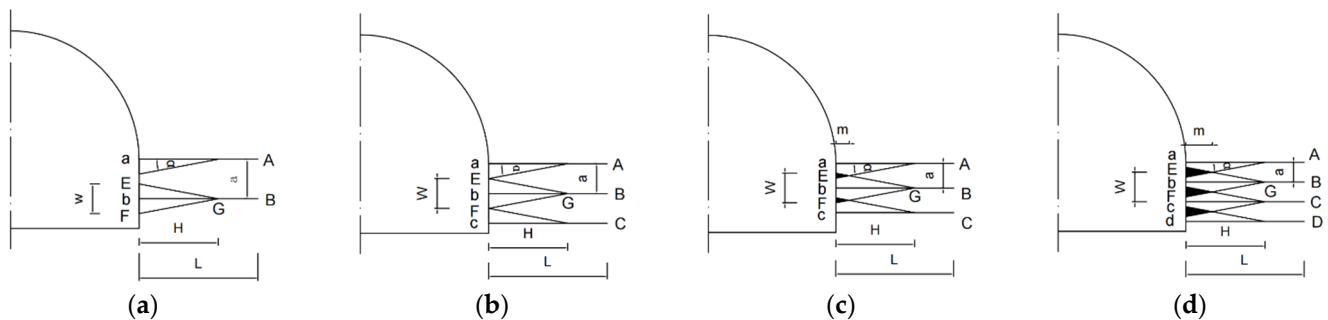


**Figure 16.** Distribution and superimposition of additional compressive stresses in multiple bolts of the surrounding rock under different bolt spacing. (a)  $800$  mm  $\times$   $800$  mm, (b)  $600$  mm  $\times$   $600$  mm, (c)  $500$  mm  $\times$   $500$  mm, (d)  $400$  mm  $\times$   $400$  mm.

With a bolt length  $L$  of  $2400$  mm and a bolt spacing  $a \times b$  of  $400$  mm  $\times$   $400$  mm, when the bolt pre-stress increases from  $F = 70$  kN to  $F = 50$  and  $90$  kN, the height of the triangle formed by the single bolt along the b-B direction almost remains constant at  $H = 1600$  mm and the superposed areas of additional compressive stress in adjacent bolts do not change significantly, while the additional compressive stress changes from  $\Delta\sigma_c = -0.117$  Mpa to  $\Delta\sigma_c = -0.088$  Mpa and  $\Delta\sigma_c = -0.149$  Mpa, indicating that the bolt pre-stress significantly affects the magnitude of additional compressive stress.

Figures 13–15 show that when bolt spacing  $a \times b$  and the applied preload  $F$  are set to  $400$  mm  $\times$   $400$  mm and  $70$  kN, respectively, as the bolt length decreases from  $L = 2400$  mm to  $L = 1500$  mm and  $2000$  mm, the corresponding height of the triangle along the b-B direction changes from  $H = 1600$  mm to  $H = 800$  mm and  $H = 1200$  mm, respectively. It is observed that the additional compressive stress in adjacent bolts has significant superposition and changes from  $\Delta\sigma_c = -0.117$  Mpa to  $\Delta\sigma_c = -0.087$  Mpa and  $\Delta\sigma_c = -0.095$  Mpa, respectively. It is inferred that the bolt length significantly affects the range of the pre-stressed bolt compression arch and the magnitude of additional compressive stress.

## 5.2. Bearing Mechanism of the Pre-Stressed Bolt Compression Arch in the Deep Soft Rock Roadway

The bearing performance of the pre-stressed bolt compression arch in the deep soft rock roadway can be analyzed based on the thickness of the compression arch and the strength of the surrounding rock induced by additional stress inside the compression arch.

### 5.2.1. Thickness of the Compression Arch

Figure 16 reveals that the compression arch thickness  $m$  can be calculated through the following expression:

$$m = H - \frac{a}{2 \tan \alpha}$$

where  $H$ ,  $a$ , and  $\alpha$  are the triangle height of a single pretension bolt, bolt spacing, and bolt stress control angle. Table 5 shows the thicknesses of the pre-stressed bolt compression arches ( $m$ ) for different bolt spacing and bolt lengths.

**Table 5.** Pre-stressed bolt compression arch thickness.

Support Parameters of the Bolt	Thickness of Pre-Stressed Bolt Compression Arch (mm)
70 kN, $a \times b = 800 \text{ mm} \times 800 \text{ mm}$ , $L = 2400 \text{ mm}$	No arch is formed
70 kN, $a \times b = 600 \text{ mm} \times 600 \text{ mm}$ , $L = 2400 \text{ mm}$	0
70 kN, $a \times b = 500 \text{ mm} \times 500 \text{ mm}$ , $L = 2400 \text{ mm}$	266.67
70 kN, $a \times b = 400 \text{ mm} \times 400 \text{ mm}$ , $L = 2400 \text{ mm}$	533.33
70 kN, $a \times b = 400 \text{ mm} \times 400 \text{ mm}$ , $L = 1500 \text{ mm}$	266.67
70 kN, $a \times b = 400 \text{ mm} \times 400 \text{ mm}$ , $L = 2000 \text{ mm}$	400

### 5.2.2. Strength of the Compression Arch

The strength of the surrounding rock after formation of the compression arch by the additional compressive stress can be calculated using the following expression:

$$\sigma_c = \Delta\sigma_c \frac{1 + \sin \varphi}{1 - \sin \varphi} + 2c \frac{\cos \varphi}{1 - \sin \varphi}$$

where the second term reflects the increase in the surrounding rock strength due to additional compressive stress ( $\Delta\sigma_c$ ), which increases cohesion  $c$  and slightly affects the friction angle  $\varphi$ . Under different support parameters of the pre-stressed bolt, the friction angle  $\varphi$  increased from  $16^\circ$  to  $17^\circ$ . Table 6 shows the strength and cohesion of the surrounding rock in the compression arch for different pre-stressed bolts with different support parameters.

**Table 6.** Strength and cohesion of the surrounding rock in the compression arch.

Support Parameters of Bolt	$\Delta\sigma_c$ (MPa)	$\sigma_c$ (MPa)	$c'$ (MPa)
70 kN, $a \times b = 800 \text{ mm} \times 800 \text{ mm}$ , $L = 2400 \text{ mm}$	-	-	-
70 kN, $a \times b = 600 \text{ mm} \times 600 \text{ mm}$ , $L = 2400 \text{ mm}$	-	-	-
70 kN, $a \times b = 500 \text{ mm} \times 500 \text{ mm}$ , $L = 2400 \text{ mm}$	-0.092	-1.489	0.551
70 kN, $a \times b = 400 \text{ mm} \times 400 \text{ mm}$ , $L = 2400 \text{ mm}$	-0.117	-1.533	0.567
50 kN, $a \times b = 400 \text{ mm} \times 400 \text{ mm}$ , $L = 2400 \text{ mm}$	-0.088	-1.482	0.548
90 kN, $a \times b = 400 \text{ mm} \times 400 \text{ mm}$ , $L = 2400 \text{ mm}$	-0.149	-1.589	0.588
70 kN, $a \times b = 400 \text{ mm} \times 400 \text{ mm}$ , $L = 1500 \text{ mm}$	0.087	-1.48	0.547
70 kN, $a \times b = 400 \text{ mm} \times 400 \text{ mm}$ , $L = 2000 \text{ mm}$	-0.095	-1.494	0.553

### 5.3. Engineering Verification and Application

The semi-circular arched roadway with a straight wall in the deep fracture zone of the west wing that returns air to the main roadway of No. 2 coal mine of Yuandian adopts the support measure of the pre-stressed bolt (cable) combined with grouting and the metal bracket shown in Figure 2. The actual field value is the same as the computer software simulation value for a pre-tightening force  $F$  of 70 kN, bolt length  $L$  of 2400 mm, and bolt spacing  $a \times b$  of 400 mm  $\times$  400 mm. Furthermore, multi-point displacement gauges were applied to measure the bolt compression arch thickness and verify the performed analysis. Figure 17 shows that several multi-point displacement gauges were placed along the arch baseline and eight bolt flukes A—H were placed at 0 m, 0.5 m, 1 m, 1.5 m, 2 m, 5 m, 7.5 m, and 10 m from the roadway surface, respectively.  $u_H$  denotes the displacement at a

depth H of the roadway surrounding rock so that the change in the length of the steel wire rope of the bolt claw at the connecting point G reflects the displacement of the roadway surface. Moreover, the difference in the displacement between points A, B, C, D, E, F, and G and the roadway surface was calculated based on the change in the length of the steel wire rope. In this regard, Figure 18 shows the correlation between the displacement of points and the distance from the roadway. It is observed that in the range of 1.5 m from the straight wall side of the roadway, the surrounding rock has translational movements, and its displacement is around 150 mm. Moreover, it is found that the thickness of the compression arch is around 500 mm, which is consistent with the result of the numerical simulation.

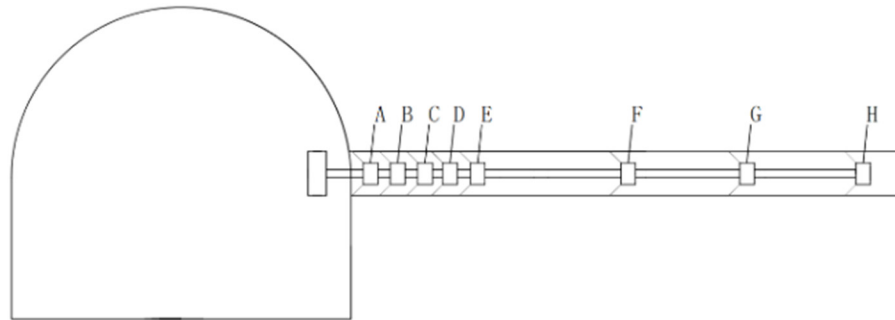


**Figure 17.** Layout of multi-point displacement gauges.

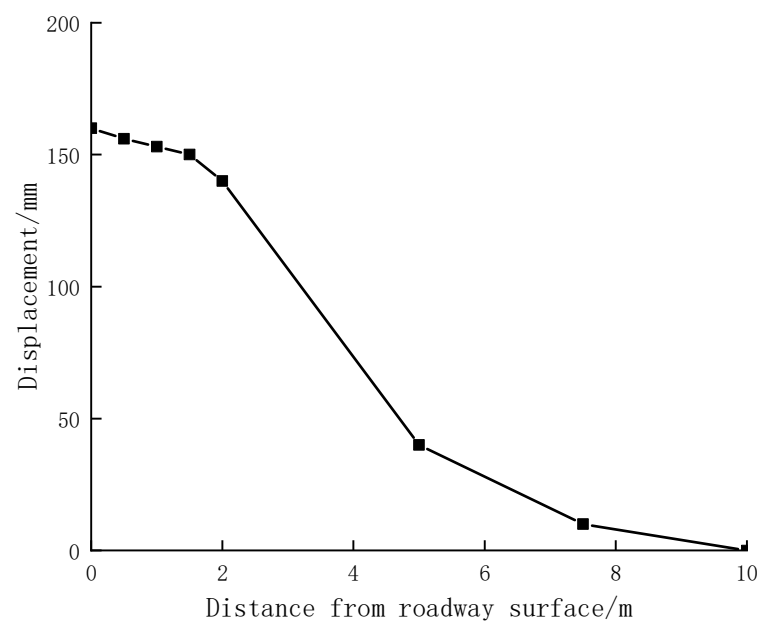


**Figure 18.** Displacement of the measuring points against the distance from the roadway surface.

Since the support plan was formulated in March 2020, as shown in Figures 19 and 20, the excavation volume of the middle coal roadway in Yuandian No.2 Coal Mine increased from an average of 475 m per month to 502 m in July, 534 m in August, 523 m in September, 505 m in October, 603 m in November, and 611 m in December, with an average increase of 71.33 m. At the same time, the maintenance amount of other extraction roadways that have been put into use has been reduced from an average of 224.83 m per month to 143 m in July, 115 m in August, 108 m in September, 95 m in October, 105 m in November, and 111 m in December, with an average reduction of 112 m. The gas extraction rate has increased by about 41% compared with that of before the new support scheme, which has promoted the safe production of coal mines and improved economic benefits.

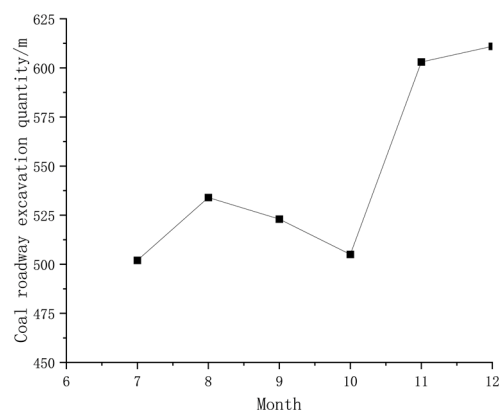


Figure 19. July to December coal roadway excavation quantity line chart.

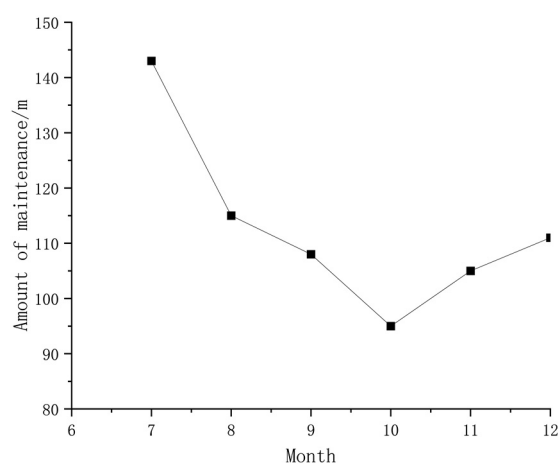


Figure 20. Extraction roadway maintenance line chart from July to December.

## 6. Conclusions

The conclusions and main achievements of this paper can be summarized as follows:

- (1) A single pre-stressed force bolt forms a triangular area with a certain range of uniform additional compressive stress distribution in the surrounding rock of a deep soft rock roadway. The interaction of multiple pre-stressed force bolts makes the additional compressive stress that is evenly distributed in the triangular area effectively superimposed to form a certain thickness and strength compression arch. The thickness and strength of the compressed arch are determined by the range and size of the uniformly distributed additional compressive stress.
- (2) The bolt spacing and bolt length significantly affect the thickness of the compression arch, and the bolt spacing, bolt length, and pre-tightening force of bolts significantly affect the strength of the compression arch. The bolt pre-tightening force  $F = 70$  kN, the length  $L = 2400$  mm, and the additional compressive stress begin to be effectively superimposed when the bolt spacing is reduced to  $a \times b = 600$  mm  $\times$  600 mm. When reducing the bolt spacing between the bolts to  $a \times b = 500$  mm  $\times$  500 mm, 400 mm  $\times$  400 mm, the thickness of the compression arch is changed from 0 mm to 266.67 mm, 533.33 mm, and the strength of the compression arch is increased from 0 MPa to  $-1.489$  MPa,  $-1.533$  MPa. The pre-tightening force of the bolt is changed to  $F = 50$  kN and 90 kN, the thickness of the compression arch is unchanged, and the strength is changed from  $-1.533$  MPa to  $-1.482$  MPa and  $-1.589$  MPa; when the length of the bolt is changed to  $L = 2000$  mm and 1500 mm, the thickness of the compression arch is changed to 400 mm and 266.67 mm, and the strength of the compression arch is changed from  $-1.533$  MPa to  $-1.494$  MPa and  $-1.48$  MPa.

- (3) The new support scheme is applied to the engineering practice of the straight wall semi-circular arch roadway in the deep fracture zone of the west wing return air roadway in Yuandian No.2 Mine. The multi-point displacement meter measures the pre-stressed anchor compression arch's displacement distribution, and the measured results are mostly consistent with the findings of the study. After the formulation of the new support scheme, the amount of coal roadway excavation increased by 71.33 m/month on average, the maintenance amount of extraction roadway decreased by 112 m/month on average, and the extraction rate increased by 41%.

**Author Contributions:** Software, N.L.; Formal analysis, N.L.; Investigation, N.L.; Writing—original draft, D.W. and N.L.; Writing—review & editing, D.W., N.L., M.H. and H.L. All authors have read and agreed to the published version of the manuscript.

**Funding:** National Natural Science Foundation of China: research on quantitative discrimination of deep coal rock stability (51374009); research on reasonable bearing mechanism and calculation theory of pre-stressed anchor cable compression arch in deep coal roadway (51674005).

**Institutional Review Board Statement:** Not applicable.

**Informed Consent Statement:** Not applicable.

**Data Availability Statement:** Not applicable.

**Conflicts of Interest:** The authors declare no conflict of interest.

## References

- Huang, W.; Zhang, K.; Tang, X.; Zhao, Z.; Wan, H. Coking Coals Potential Resources Prediction in Deep Coal Beds in Northern China. *Energy Explor. Exploit.* **2010**, *28*, 313–325. [\[CrossRef\]](#)
- Li, D.; Cheng, Y. Evaluation of Gas Control Ability of a Coal and Gas Outburst Mine. *Energy Sources Part A Recovery Util. Environ. Eff.* **2014**, *36*, 2401–2409. [\[CrossRef\]](#)
- Lu, S.; Li, L.; Cheng, Y.; Sa, Z.; Zhang, Y.; Yang, N. Mechanical failure mechanisms and forms of normal and deformed coal combination containing gas: Model development and analysis. *Eng. Fail. Anal.* **2017**, *80*, 241–252. [\[CrossRef\]](#)
- Xinfeng, W.; Yiyang, Z.; Qiao, Z.; Youyu, W.; Wengang, L.; Tian, J. Space-Time Evolution Characteristics of Deformation and Failure of Surrounding Rock in Deep Soft Rock Roadway. *Sustainability* **2022**, *14*, 12587. [\[CrossRef\]](#)
- Hao, T.; Xiang, J.; Hongyi, Z.; Tianbin, L. Numerical simulation of large compression deformation disaster and supporting behavior of deep buried coal rock tunnel with high in situ stress based on CDEM. *Adv. Civ. Eng.* **2022**, *2022*, 5985165.
- Zhang, J.; Liu, L.; Liu, C.; Li, Y. Mechanism and application of new prestressed yield bolt for controlling deep high-stress rock mass. *Tunn. Undergr. Space Technol.* **2022**, *119*, 104254.
- Bo, W.; Wei, Y.; Ziquan, C. Effect of bolt plate on the mechanical behavior of prestressed rock bolt used in squeezing large deformation tunnel. *Acta Geotech.* **2022**, *17*, 3591–3611.
- Xiaowei, G.; Xigui, Z.; Peng, L.; Rui, L.; Cancan, L.; Muhammad, S.N.; Cong, W.; Boyang, L.; Wenjie, X.; Guowei, L. Full-stress bolting technology and application of bolts in the coal roadway. *Energies* **2021**, *14*, 7475.
- Xiaowei, F.; Nong, Z.; Fengzhen, H.; Sen, Y.; Xigui, Z. Implementation of a pretensioned, fully bonded bolting system and its failure mechanism based on acoustic emission: A laboratorial and field study. *Geotech. Test. J.* **2017**, *40*, 978–999.
- Kai, W.; Baogui, Y.; Zhongkui, W.; Xiaolong, W. Analytical solution for the deformation and support parameters of coal roadway in layered roof strata. *Geofluids* **2021**, *2021*, 6669234.
- Zhang, Q.; Jiang, B.; Wang, S.; Ge, X.; Zhang, H. Elasto-plastic analysis of a circular opening in strain-softening rock mass. *Int. J. Rock Mech. Min. Sci.* **2012**, *50*, 38–46. [\[CrossRef\]](#)
- Minggao, Q.; Pingwu, S.; Jialin, X. *Mine Pressure and Rock Strata Control*; China University of Mining and Technology Press: Xuzhou, China, 2010; pp. 25–26.
- Mohammadi, M.; Hossaini, M.F.; Bagloo, H. Rock bolt supporting factor: Rock bolting capability of rock mass. *Bull. Eng. Geol. Environ.* **2017**, *76*, 231–239. [\[CrossRef\]](#)
- Li, S.-c.; Wang, H.-t.; Wang, Q.; Jiang, B.; Wang, F.-q.; Guo, N.-b.; Liu, W.-j.; Ren, Y.-x. Failure mechanism of bolting support and high-strength bolt-grouting technology for deep and soft surrounding rock with high stress. *J. Cent. South Univ.* **2016**, *23*, 440–448. [\[CrossRef\]](#)
- Zhang, Q.-H.; Liu, Q.-B.; Wang, S.-H.; Liu, H.-L.; Shi, G.-H. Progressive failure of blocky rock system: Geometrical-mechanical identification and rock-bolt support. *Rock Mech. Rock Eng.* **2022**, *55*, 1649–1662. [\[CrossRef\]](#)
- Kun, Z.; Jinpeng, S.; Zengkai, L.; Hongyue, C.; Qiang, Z.; Shaoan, S. Sensitivity analysis and experimental verification of bolt support parameters based on orthogonal experiment. *Shock Vib.* **2020**, *2020*, 8844282.

17. Li, N.; Wang, F.; Song, G. Monitoring of bolt looseness using piezoelectric transducers: Three-dimensional numerical modeling with experimental verification. *J. Intell. Mater. Syst. Struct.* **2020**, *31*, 911–918. [[CrossRef](#)]
18. Wang, Z.; Fei, C.-W.; Wang, J.-J. Equivalent simulation of mechanical characteristics for parametric modeling of bolted joint structures. *Adv. Mech. Eng.* **2017**, *9*, 1687814017704360. [[CrossRef](#)]
19. Wang, X.-Y.; Zhu, S.-F.; Wang, X.; Zhang, X.-C. Stress and thickness calculation of a bolted flat cover with double metal sealing rings. *Nucl. Sci. Tech.* **2018**, *29*, 120. [[CrossRef](#)]
20. Chen, Y.; Wen, G.; Hu, J. Analysis of Deformation Characteristics of Fully Grouted Rock Bolts Under Pull-and-Shear Loading. *Rock Mech. Rock Eng.* **2020**, *53*, 2981–2993. [[CrossRef](#)]

**Disclaimer/Publisher's Note:** The statements, opinions and data contained in all publications are solely those of the individual author(s) and contributor(s) and not of MDPI and/or the editor(s). MDPI and/or the editor(s) disclaim responsibility for any injury to people or property resulting from any ideas, methods, instructions or products referred to in the content.